CGMS-XXXII EUM-WP-12
Prepared by EUMETSAT
Agenda Item: 11/2

EVALUATION OF THE MSG/SEVIRI SOLAR CHANNELS CALIBRATION REFERENCE WITH RESPECT TO OTHER RADIOMETERS

The operational absolute calibration of SEVIRI solar channels relies on modelled radiances over bright desert sites, as no in-flight calibration device is available. These simulated radiances represent therefore the "reference" against which SEVIRI is calibrated. This document evaluates the uncertainties associated with the characterization of this "reference", *i.e.*, the modelled radiances. To this end, top-of-atmosphere simulated radiances are compared with several thousands of calibrated satellite observations. This paper has been written in response to CGMS action 31.26.

1 INTRODUCTION

The calibration MSG/SEVIRI solar channels relies on radiative transfer modelling over bright desert. These simulated radiances represent therefore the "reference" against which these channels are calibrated. The objective of this paper is to evaluate the accuracy of the SEVIRI calibration "reference". This evluation is based on a comparison between simulated radiances with calibrated observations acquired by spaceborne instruments such as the Along-Track Scanning Radiometer (ATSR-2 and AATSR) instruments of the European Space Agency (ESA) flying respectively on the European Remote Sensing Satellite-2 (ERS-2) and ENVIronmental Research SATellite (ENVISAT), the Sea-viewing Wide Field-of-view Sensor (SeaWiFS) instrument on board the National Aeronautics and Space Administration (NASA) SeaStar spacecraft, the VEGETATION instrument on the french "Système pour l'Observation de la Terre" (SPOT-4) platform and finally the MEdium Resolution Imaging Spectrometer (MERIS) flying on ENVISAT.

Table 1: SEVIRI Solar Channel Characteristics. The dynamic range is given in $\mathrm{Wm}^{-2}\mathrm{sr}^{-1}\mu\mathrm{m}^{-1}$. The Signal to Noise Ratio (SNR) is given at 1% of the maximum dynamic range. The standard deviation (std. d.) of the Normalized Spectral Response (NSR) characterization error is given in percent. The calibration requirement is given in $\mathrm{Wm}^{-2}\mathrm{sr}^{-1}\mu\mathrm{m}^{-1}$.

Channel	Spectral Band (μm)	Dynamic Range	Short-term Noise Perf.	NSR std. d.	Cal. Requ.
HRV	0.37 – 1.25	0 – 460	SNR$>$ 4.6	1.8%	9.18
VIS0.6	0.56 – 0.71	0 – 533	SNR$>$14.3	1.0%	10.66
VIS0.8	0.74 – 0.88	0 – 357	SNR$>$ 9.7	1.0%	7.14
NIR1.6	1.50 – 1.78	0 – 75	SNR$>$ 3.0	0.8%	1.50

2 THE SEVIRI RADIOMETER

SEVIRI is the main radiometer on board the MSG spacecraft. It scans the Earth disc every 15 minutes within 11 spectral channels located between 0.6μm and 14μm and a high resolution broadband visible channel (HRV). The East-West and South-North sampling distance at the sub-satellite point is 3$\times$3 km (1$\times$1 km for HRV), and the instantaneous field of view is about 5km (2km for HRV). The characteristics of the channels located in the solar spectral region are given in Table (1), where the actual pre-launch radiometric performances are given for the SEVIRI instrument onboard MSG-1. Each spectral channel is composed of three detectors, except HRV with nine. The output signal of all channels is coded on 10 bits. The medium-term (long-term) drift is expected to be better or equal to 0.1% (2%) of the maximum dynamic range. The normalized spectral response $\xi(\lambda)$ of the solar channels is characterized with a mean relative error of about 1%, which represents a significant improvement with respect to the VIS band of the Meteosat first generation radiometer. The sensor spectral responses (SSR) and associated error are shown on Fig. (1). The SSR total error accounts for errors due to the absolute wavelength calibration uncertainty, the measurement noise and bias of the optic and detector transmittance.

The radiometric preprocessing of level 1.0 data, *i.e.*, the transformation of raw data to level 1.5 geo-located radiances, includes the linearization of the signal, the equalization of the detector output of a same channel and finally the pixel geo-location to a reference grid centered at 0 degree longitude (Schmetz et al. 2002). The image size is 3712$\times$3712 pixels except for the HRV band which has a size of 11136$\times$5568 (SN$\times$EW). The geo-location absolute accuracy is expected to be about one pixel with a root mean square error from image to image less than 0.5 pixel. Ground control points are used to monitor the quality of the geo-location process.

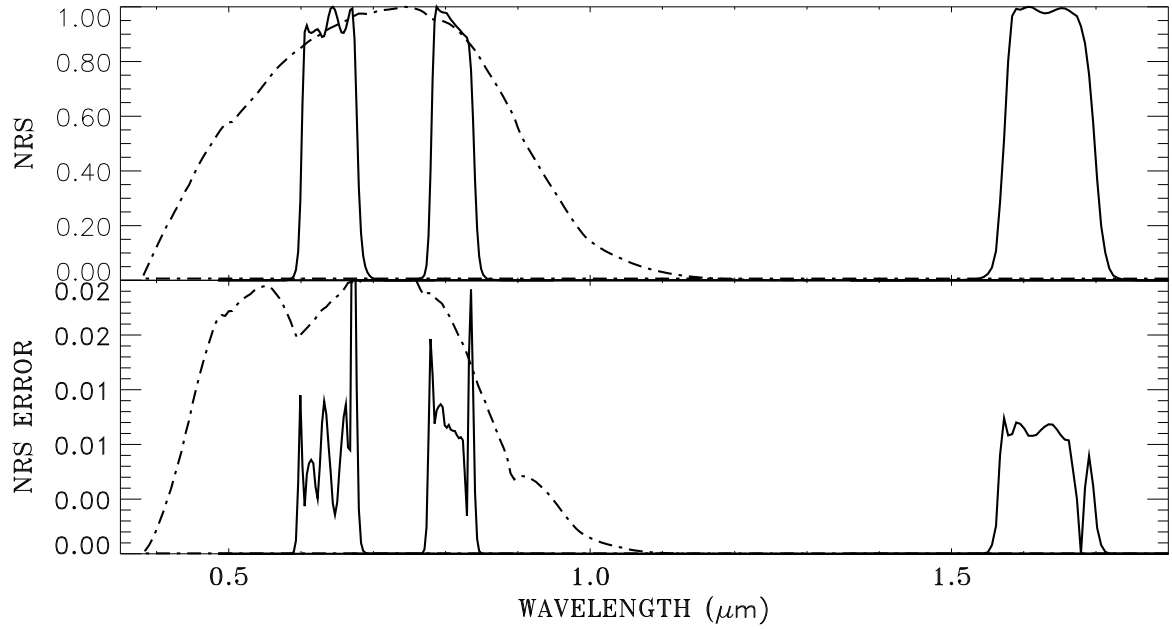

Figure 1: Top: Normalized Spectral Response (NSR) of the SEVIRI solar channels. The response of the HRV band is shown with a dash-dotted line. Bottom: NSR characterization absolute error.

3 CALIBRATION TARGET CHARACTERIZATION

The main reference for the calibration of the SEVIRI solar channels consists of simulated TOA spectral radiances over bright desert targets. The spectral radiance $R(\chi_d, \lambda; \chi_p)$ impinging on a spaceborne instrument at the wavelength λ is determined by a set of independent parameters $\{\chi_d\}$ that define the observation conditions and a set of state variables $\{\chi_p\}$ that describe the radiative properties of the observed targets, *i.e.*, the atmosphere and the underlying surface. The independent parameters include the sun and viewing angles, the time of observation and finally the target location. Hence, the bulk effort concerning the "calibration reference" determination essentially consists in the characterization of the radiative transfer model state variables. The bright desert targets are described in Govaerts and Clerici (2004).

Table 2: Selected spectral bands for each instrument.

BAND		MERIS	ATSR-2	AATSR	SeaWiFS	VGT
BLUE	440	442	–	–	443	B0
GREEN	550	560	550	550	555	–
RED	670	665	660	660	670	B2
NIR	870	865	870	870	865	B3
SWIR	1600	–	1600	1600	–	MIR

4 CALIBRATION REFERENCE EVALUATION

4.1 Method

As stated in the introduction, the objective of this evaluation is to assess the accuracy and precision of the SEVIRI calibration reference, *i.e.*, simulated TOA radiances. Since the surface and atmospheric properties are

characterized in the entire 0.35 – 1.8μm interval, it is possible to simulate spectral radiance at any wavelengths within that spectral range. In particular, if the description of the target is reliable, it should be possible to realistically simulate any passive spaceborne observations acquired in that spectral domain. The proposed evaluation method relies thus on the simulation of calibrated observations $\widetilde{R}^*_f(\chi_d)$ acquired by polar orbiting instruments over the desert sites. Calibrated time series have been collected over the calibration sites in the blue, green, red, near infrared (NIR) and 1.6 μm spectral region (Table 2). The acquisition period (Table 5) and the preparation of these time series differ for each instrument. These observations are averaged over a 100 km $\times$ 100 km areas centered on each target location but SeaWiFS with an area of about 20 km $\times$ 20 km. The standard deviation $\sigma_{\widetilde{R}^*_f}$ of $\widetilde{R}^*_f$ over these targets usually does not exceed 2%. These observations are next simulated accounting for the exact geometry of observation and illumination as well as the spectral response $\xi_f(\lambda)$ of each simulated band. These calculated effective radiances write

$$\widetilde{R}_f(\chi_d;\chi_p) = \frac{\int_\lambda R(\chi_d,\lambda;\chi_p)\,\xi(\lambda)\,d\lambda}{\int_\lambda \xi(\lambda)\,d\lambda} \tag{1}$$

The corresponding simulation error $\delta\widetilde{R}_f(\chi_d;\chi_p)$ is calculated accounting for the estimated state variable characterization error ϵ_p. The comparisons between observations and simulations are based on the analysis of the following values:

1. The relative bias $\beta(t,d)$ between simulation and observation acquired over target d at time t is estimated with
$$\beta(t,d) = \frac{\widetilde{R}^*_f(t,d;\chi_p) - \widetilde{R}_f(t,d;\chi_p)}{\widetilde{R}_f(t,d;\chi_p)} \tag{2}$$
where $\widetilde{R}^*_f(t,d)$ is the observed radiance averaged over the target area and $\widetilde{R}_f(t,d;\chi_p)$ the simulated radiance with the target properties χ_p.

2. The bias error $\delta\beta(t,d)$ equals to
$$\delta\beta(t,d) = \beta(t,d)\sqrt{\left(\frac{\delta\widetilde{R}^*_f(t,d;\chi_p)}{\widetilde{R}^*_f(t,d;\chi_p)}\right)^2 + \left(\frac{\delta\widetilde{R}_f(t,d;\chi_p,\varepsilon_p)}{\widetilde{R}_f(t,d;\chi_p)}\right)^2} \tag{3}$$
and $\delta\widetilde{R}^*_f(d,t)$ is the observation error. This error is equal to the standard deviation of the pixels covering the desert site area, neglecting for the time being possible systematic errors due to instrument calibration uncertainties.

3. The monthly mean relative weighted bias $\overline{\beta}_m$ over all 18 targets
$$\overline{\beta}_m = 100\frac{1}{18}\sum_{d=1}^{18} W_\beta \sum_{t\in T_m} \frac{\beta(t,d)}{\delta\beta^2(t,d)} \tag{4}$$
where $W_\beta = \sum_{t\in T_m} \delta\beta^2(t,d)$.

4. The standard deviation $\sigma_{\overline{\beta}_m}$ of $\overline{\beta}_m(d)$.

5. The relative bias averaged over the entire period $\overline{\beta}$.

6. The standard deviation $\sigma_{\overline{\beta}}$ of $\overline{\beta}$.

7. The correlation coefficient r between simulation and observations is calculated as an estimate of the reliability of the method. A high correlation should be expected when both satellite data and observation simulations $\widetilde{R}_f(\chi_d;\chi_p)$ are correct.

The quantity $\overline{\beta}$ represents an estimate of our calibration reference accuracy over a given period of time with respect to a specific instrument. The precision of this estimate is given by the standard deviation $\sigma_{\overline{\beta}_m}$ of $\overline{\beta}_m$.

Similar statistics are derived with respect to Bidirecional Reflectance Factor (BRF) instead of the effective radiance.

4.2 Results

Table 3: Comparison between observations and simulated radiance. r is the correlation coefficient. $\overline{\beta}_m$ is the mean relative bias in percent. $\sigma_{\overline{\beta}_m}$ is the standard error of $\overline{\beta}_m$.

BAND	440			550			670			870			1600		
SENSOR	r	$\overline{\beta}$	$\sigma_{\overline{\beta}}$	r	$\overline{\beta}$	$\sigma_{\overline{\beta}}$	r	$\overline{\beta}$	$\sigma_{\overline{\beta}}$	r	$\overline{\beta}$	$\sigma_{\overline{\beta}}$	r	$\overline{\beta}$	$\sigma_{\overline{\beta}}$
ATSR2	–	–	–	0.92	1.9	6.7	0.98	4.0	3.6	0.98	3.9	3.0	0.99	0.3	1.5
AATSR	–	–	–	0.97	9.3	5.4	0.98	9.6	3.3	0.98	19.4	3.2	0.97	-10.5	4.1
SEAWIFS	0.95	2.0	4.6	0.93	-2.3	4.9	0.97	-0.2	2.9	0.97	1.1	2.8	–	–	–
VGT	0.96	0.5	4.5	–	–	–	0.98	4.9	2.6	0.98	5.2	2.8	0.92	-4.1	2.7
MERIS	0.95	7.9	5.2	0.92	0.1	4.5	0.98	3.0	1.6	0.98	6.3	1.7	–	–	–
SEVIRI	–	–	–	–	–	–	0.99	-1.9	2.7	0.99	-0.6	2.8	0.99	-0.8	3.9

Table 4: Comparison between observations and simulated BRF. r is the correlation coefficient. $\overline{\beta}_m$ is the mean relative bias in percent. $\sigma_{\overline{\beta}_m}$ is the standard error of $\overline{\beta}_m$.

BAND	440			550			670			870			1600		
SENSOR	r	$\overline{\beta}$	$\sigma_{\overline{\beta}}$	r	$\overline{\beta}$	$\sigma_{\overline{\beta}}$	r	$\overline{\beta}$	$\sigma_{\overline{\beta}}$	r	$\overline{\beta}$	$\sigma_{\overline{\beta}}$	r	$\overline{\beta}$	$\sigma_{\overline{\beta}}$
ATSR2	–	–	–	0.75	4.2	6.6	0.88	4.6	3.4	0.89	3.3	3.1	0.95	-1.1	1.6
AATSR	–	–	–	0.93	8.1	5.3	0.93	8.6	3.2	0.93	9.8	3.0	0.72	-10.1	4.1
SEAWIFS	0.96	0.1	4.5	0.88	-1.7	4.9	0.94	-0.3	2.9	0.94	-2.5	2.8	–	–	–
VGT	0.95	1.4	4.6	–	–	–	0.95	4.8	2.5	0.93	3.9	2.7	0.68	-5.0	2.7
MERIS	0.95	4.9	5.1	0.91	3.0	4.6	0.98	4.4	1.6	0.98	5.5	1.6	–	–	–
SEVIRI	–	–	–	–	–	–	0.92	-1.9	2.7	0.92	-0.6	2.8	0.73	-0.8	3.9

Table 5: Acquisition period (month number and year) and number of clear sky observations over each calibration target for each instrument.

TID	ATSR2		AATSR		SEAWIFS		VGT		MERIS		SEVIRI	
ALG1	– – –	–	– – –	–	11/1999 – 01/2002	550	04/1998 – 08/2002	672	08/2002 – 06/2003	9	– – –	–
ALG2	– – –	–	– – –	–	11/1999 – 01/2002	495	04/1998 – 08/2002	705	07/2002 – 10/2002	8	– – –	–
ALG3	05/1995 – 06/1997	208	10/2002 – 07/2003	29	11/1999 – 02/2002	712	04/1998 – 08/2002	782	07/2002 – 09/2003	26	02/2003 – 12/2003	294
ALG4	03/1997 – 05/1997	8	– – –	–	11/1999 – 02/2002	640	04/1998 – 08/2002	789	07/2002 – 09/2003	21	02/2003 – 12/2003	367
ALG5	11/1996 – 06/1997	18	10/2002 – 07/2003	32	11/1999 – 03/2002	681	04/1998 – 08/2002	730	08/2002 – 09/2003	24	02/2003 – 12/2003	452
ARA1	06/1995 – 06/1997	256	10/2002 – 07/2003	14	10/1997 – 02/2002	808	04/1998 – 08/2002	781	07/2002 – 08/2003	21	07/2003 – 12/2003	118
ARA2	11/1996 – 05/1997	19	– – –	–	10/1997 – 02/2002	929	06/1998 – 08/2002	674	07/2002 – 08/2003	23	07/2003 – 12/2003	15
SUD1	06/1995 – 01/2001	411	10/2002 – 07/2003	33	10/1997 – 02/2002	436	12/2000 – 08/2002	766	07/2002 – 08/2003	30	07/2003 – 12/2003	323
NIG1	11/1996 – 06/1997	34	– – –	–	11/1999 – 01/2002	256	12/2000 – 08/2002	652	07/2002 – 08/2003	22	02/2003 – 12/2003	439
NIG2	11/1996 – 06/1997	36	– – –	–	11/1999 – 01/2002	330	12/2000 – 08/2002	670	07/2002 – 08/2003	38	02/2003 – 12/2003	419
NIG3	11/1996 – 06/1997	20	– – –	–	11/1999 – 01/2002	223	12/2000 – 08/2002	669	07/2002 – 08/2003	28	02/2003 – 12/2003	118
EGY1	– – –	–	– – –	–	10/1997 – 02/2002	611	04/1998 – 08/2002	872	07/2002 – 10/2002	11	– – –	–
LIB1	05/1995 – 06/1997	161	10/2002 – 07/2003	30	01/2000 – 12/2001	327	04/1998 – 08/2002	762	07/2002 – 08/2003	25	02/2003 – 11/2003	223
LIB2	11/1996 – 06/1997	27	10/2002 – 07/2003	29	11/1999 – 12/2001	460	04/1998 – 08/2002	684	08/2002 – 08/2003	32	07/2003 – 12/2003	180
LIB3	11/1996 – 06/1997	132	– – –	–	11/1999 – 12/2001	308	04/1998 – 08/2002	733	07/2002 – 09/2003	38	07/2003 – 12/2003	294
LIB4	– – –	–	– – –	–	11/1999 – 11/2001	574	04/1998 – 08/2002	732	07/2002 – 10/2002	11	– – –	–
MAL1	– – –	–	– – –	–	11/1999 – 01/2002	506	12/2000 – 08/2002	532	08/2002 – 10/2002	4	– – –	–
MAU2	– – –	–	– – –	–	11/1999 – 01/2002	511	12/2000 – 08/2002	235	07/2002 – 10/2002	7	– – –	–

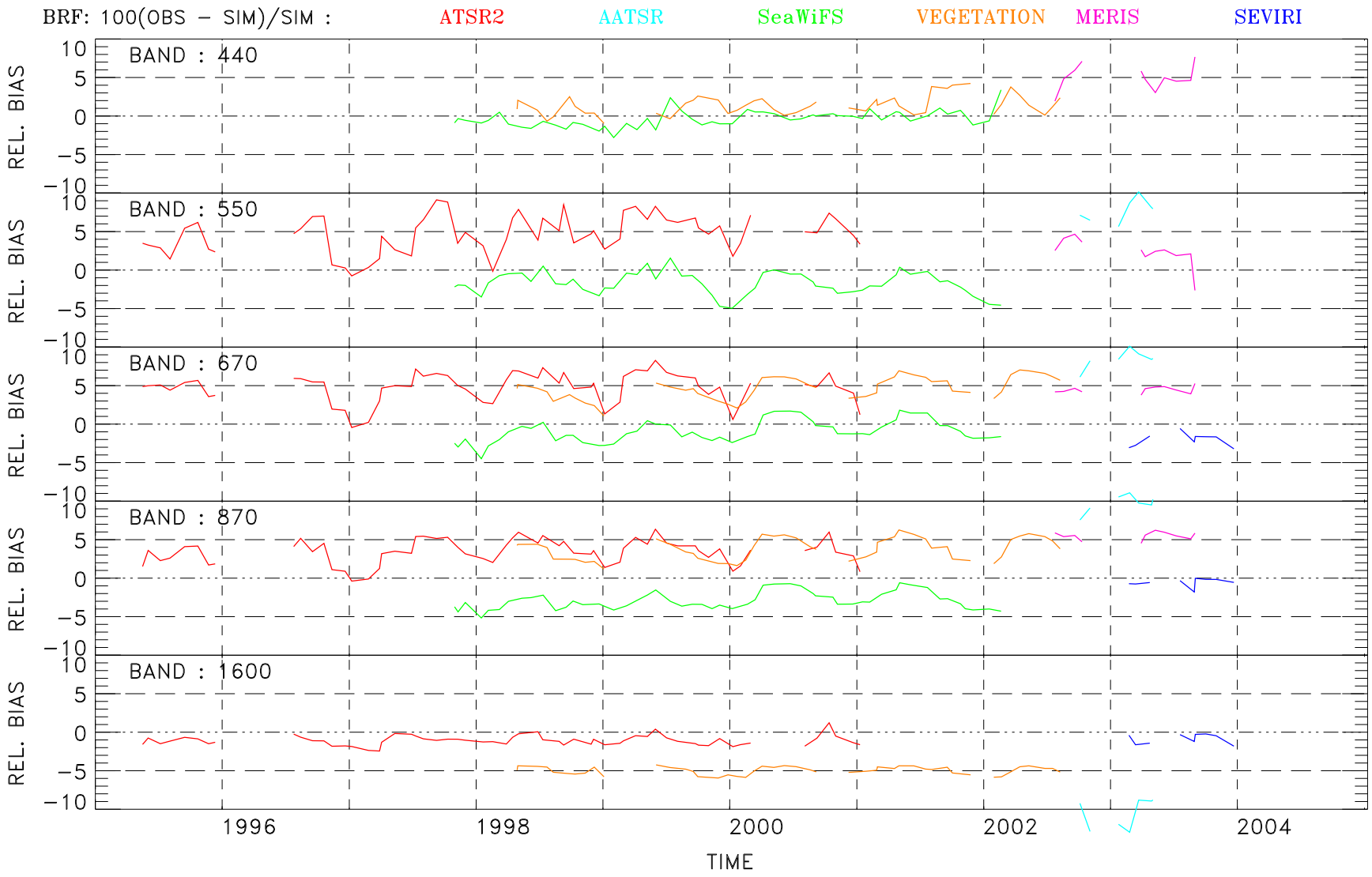

Figure 2: Monthly mean relative bias between observations and simulated radiances averaged over all desert targets in the blue, green, red, NIR and SWIR spectral regions. The standard deviation is shown with the vertical bars. The sensors are given the following color codes: ATSR-2 is in red, AATSR is in light blue, SeaWiFS in green, SPOT-4/VEGETATION in orange, MERIS in purple and SEVIRI in blue.

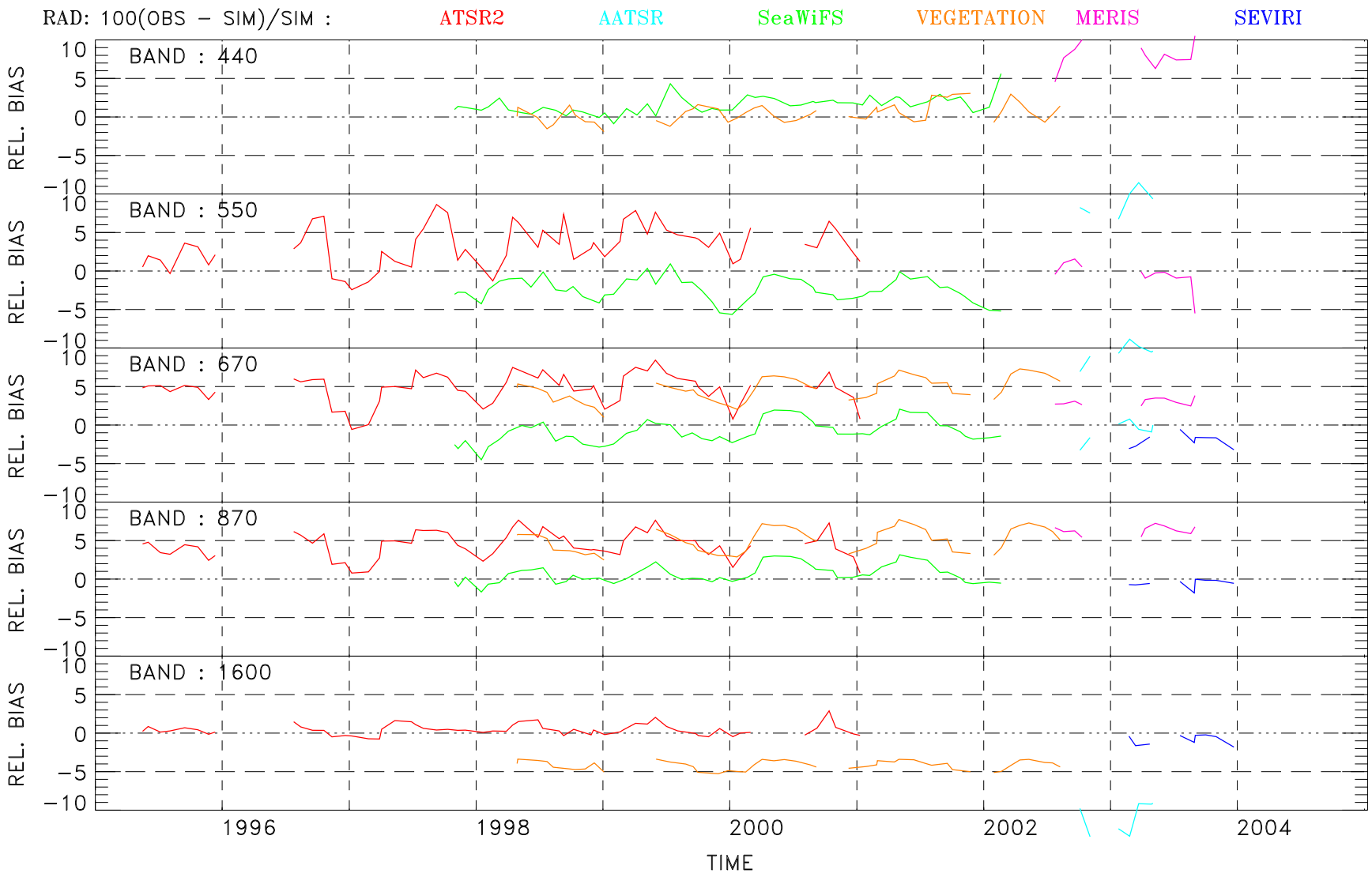

Figure 3: As Fig. (2) but with respect to the TOA BRF.

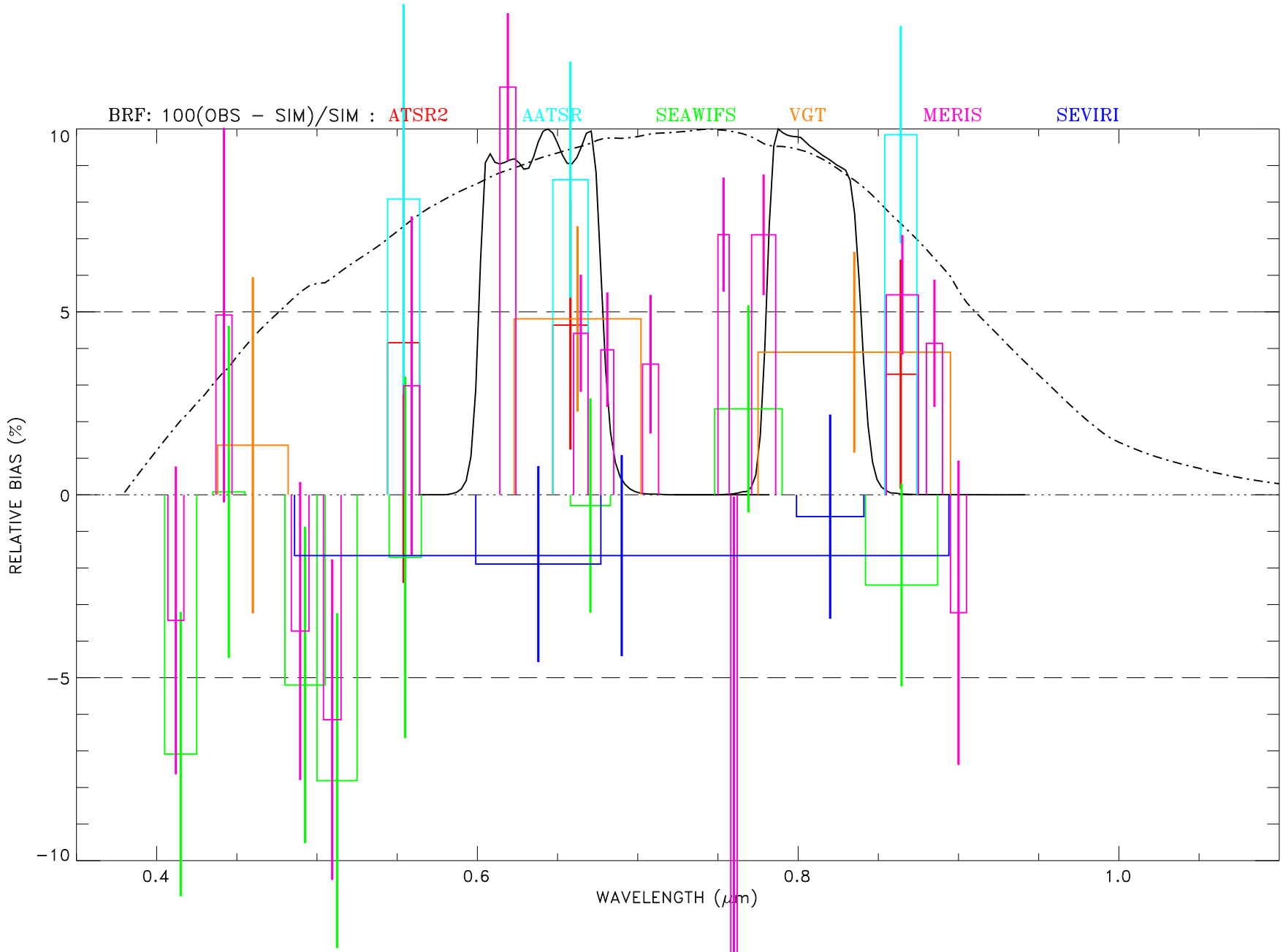

Figure 4: Mean relative bias between observations and simulated radiances averaged over all desert targets in all spectral bands available. The standard deviation is shown with the vertical bars. The sensors are given the following color codes: ATSR-2 is in red, AATSR is in light blue, SeaWiFS in green, SPOT-4/VEGETATION in orange, MERIS in purple and SEVIRI in blue.

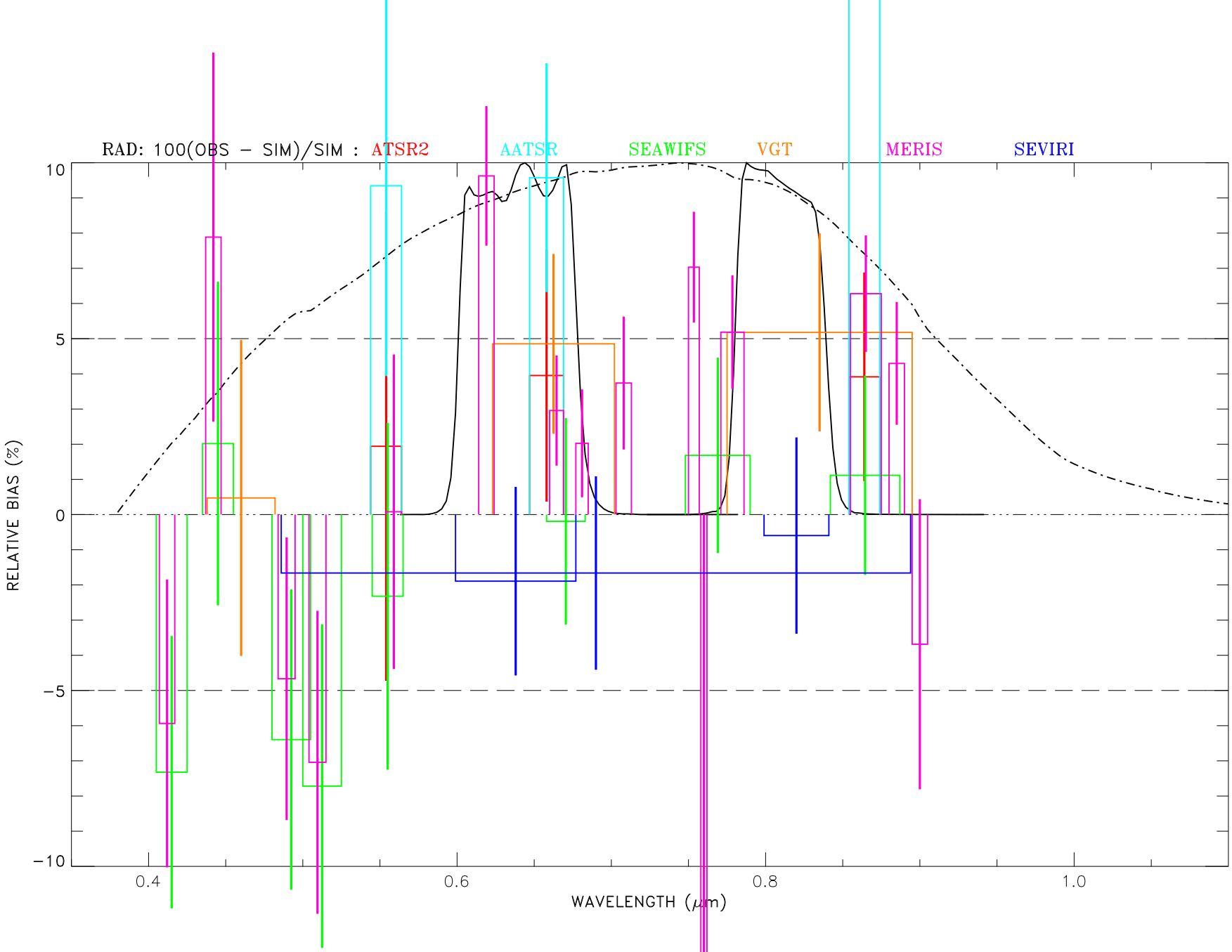

Figure 5: As Fig. (4) but with respect to the TOA BRF.

5 CONCLUSION

The calibration reference used for the operational vicarious calibration of the SEVIRI solar channels consists of simulated TOA radiances over bright desert targets, using a data set of surface and atmospheric properties. The accuracy and precision evaluation of this reference relies on a comparison between calibrated spaceborne data and their simulation. Excluding the AATSR results, these comparisons reveal that the relative bias between simulations and calibrated observations is in the range -0.2 – +4.9%in the VIS0.6 and +1.1 – +6.3% in the VIS0.8 bands. In these two bands, ATSR2, VGT1 and MERIS results are similar and suggests that SEVIRI radiances are underestimated by about 4% in the VIS0.6 band and 5% in the VIS0.8 one. Conversely, there is no significant bias between SEVIRI and SeaWiFS in these two bands.

References

Govaerts, Y. M. and M. Clerici (2004). Evaluation of radiative transfer simulations over bright desert calibration sites. *IEEE Transactions on Geoscience and Remote Sensing 42*, 176–187.

Schmetz, J., P. Pili, S. Tjemkes, D. Just, J. Kerkmann, S. Rota, and A. Ratier (2002). An introduction to Meteosat Second Generation. *Bulletin of the American Meteorological Society 83*, 977–992.